Yeast increases glycolytic flux to support higher growth rates accompanied by decreased metabolite regulation and lower protein phosphorylation

PNAS RESEARCH ARTICLE | BIOPHYSICS AND COMPUTATIONAL BIOLOGY OPEN ACCESS

Yeast increases glycolytic flux to support higher growth rates accompanied by decreased metabolite regulation and lower protein phosphorylation

Min Chen[a], Tingting Xie[a], Huan Li[a], Yingping Zhuang[a], Jianye Xia[a,b,1], and Jens Nielsen[c,d,1]

Contributed by Jens Nielsen; received February 17, 2023; accepted May 17, 2023; reviewed by Jack T. Pronk and Markus Ralser

Supply of Gibbs free energy and precursors are vital for cellular function and cell metabolism have evolved to be tightly regulated to balance their supply and consumption. Precursors and Gibbs free energy are generated in the central carbon metabolism (CCM), and fluxes through these pathways are precisely regulated. However, how fluxes through CCM pathways are affected by posttranslational modification and allosteric regulation remains poorly understood. Here, we integrated multi-omics data collected under nine different chemostat conditions to explore how fluxes in the CCM are regulated in the yeast *Saccharomyces cerevisiae*. We deduced a pathway- and metabolism-specific CCM flux regulation mechanism using hierarchical analysis combined with mathematical modeling. We found that increased glycolytic flux associated with an increased specific growth rate was accompanied by a decrease in flux regulation by metabolite concentrations, including the concentration of allosteric effectors, and a decrease in the phosphorylation level of glycolytic enzymes.

yeast | omics integration | Crabtree effect | metabolism

Significance

Flux through a pathway can be regulated by activity of the corresponding enzyme. However, to what extent a change in reaction flux can be explained by the corresponding enzyme's activity, particularly by protein phosphorylation and allosteric regulation, remains elusive. Here, we try to decipher how flux in the central carbon metabolism (CCM) is regulated by protein phosphorylation and allosteric effectors using *Saccharomyces cerevisiae* as a model organism. We find that metabolite concentration has more control over reaction flux under respiratory conditions, while it loses power under respiro-fermentative conditions. We also find that decreasing phosphorylation of glycolytic enzymes is associated with increasing fluxes across an extensive dynamic range. Our results provide insights into eukaryote metabolic regulation, especially for the CCM pathways.

Optimizing intracellular fluxes by modulating the expression of enzymes to acquire maximal titer, yield, and rate is a critical step for cell factory construction (1). To realize this goal, an iterative "design—built—test—learn" cycle has been proposed to redirect metabolic fluxes toward the desired product of interest (2). At the beginning of the cycle, the design's principle depends on properly comprehending the intracellular complicated regulatory networks. While system biology has introduced a large amount of multi-omics data to address this question, directly applying these data to make informed decisions on strain improvements is still challenging as our knowledge of metabolic flux regulation mechanisms is limited (1, 3).

Different regulatory factors can change flux through a pathway or an enzyme-catabolized reaction. For example, flux through a given reaction can be determined by the abundance and activity of the enzyme that catalyzes the reaction (4–7). However, it remains unclear how much flux change can be explained by enzyme abundance or enzyme activity (7). On the one hand, flux changes seem tightly intertwined with enzyme abundance, especially in signaling and metabolism-regulating transcriptional networks (8, 9). On the other hand, it is also reported that enzyme phosphorylation levels or metabolite concentrations correlate much better with metabolic fluxes than enzyme expression levels (5, 10). These results indicate that enzyme activity plays a dominant role in flux regulation. Therefore, it is necessary to propose an effective method to dissect the complex relationships among these regulatory factors.

Hierarchical regulation analysis seems an excellent solution to tackle this issue, as the different regulatory factors contributed to flux changes can be quantified. This method employs the regulation coefficient (ρ_i) to quantify the relative contribution of changes in each regulatory factor (transcription, posttranscription, protein abundance, thermodynamics potential, metabolite concentration, and posttranslation modification) to the flux changes (11, 12). Theoretically, if ρ_i equals one, a regulatory event that links to a specific regulatory factor (i) changes take a function (called functional regulatory events in this study) (12). Considering measurement error in the data, Gerosa et al. expanded the boundary for identifying functional regulatory events to $0.5 < \rho_i < 2$ (12). Using this theory, researchers have revealed that metabolic fluxes in the Embden–Meyerhof–Parnas (EMP) pathway are predominantly regulated at posttranscriptional levels. In contrast, the tricarboxylic acid (TCA) cycle pathway fluxes are regulated mainly by the pathway enzymes' expression level (4, 11–13).

Understanding the regulation of metabolism shifting (respiration vs. respiro-fermentation) of *Saccharomyces cerevisiae* is crucial for deciphering the mechanism behind the Crabtree

Competing interest statement: The authors disclose stock ownership in Elypta AB, Chrysea Inc., and Melt&Marble AB, but none of these companies have business related to this research. The authors are inventors of several patents/patent applications, but none related to this research.

[1]To whom correspondence may be addressed. Email: xiajy@tib.cas.cn or nielsenj@chalmers.se.

This article contains supporting information online at https://www.pnas.org/lookup/suppl/doi:10.1073/pnas.2302779120/-/DCSupplemental.

Published June 12, 2023.

effect. Many studies have been carried out, and the metabolism state is controlled cooperatively or antagonistically by different regulatory factors when cultured aerobically under limited or excess glucose. For example, the differences in the affinity constant to pyruvate between pyruvate dehydrogenase (PDH) and pyruvate decarboxylase (PDC) prompt more flux to be allocated to the fermentation pathway following a sugar pulse (14, 15). In addition, increasing the flux through pyruvate carboxylase (PYC) can also lead to an increased rate of ethanol formation via PDC (15). Moreover, repression of expression of genes involved in the oxidative metabolism and TCA cycle by higher glucose plays a critical role in switching to respiro-fermentative metabolism (16). Studies from system level analysis also report that metabolite concentration seems dominant for regulating the flux through the EMP pathway under respiratory conditions, while enzyme abundance takes over control for the same pathway under respiro-fermentative conditions (17). However, the effects of allosteric regulation and posttranslational modifications of the enzyme have not been quantified, which are crucial for flux regulation (18–20).

In this study, we addressed how flux changes through the central carbon metabolism (CCM) pathway of *S. cerevisiae* are regulated by different factors when cultured under glucose-limited chemostats at nine different dilution rates. We first quantified the metabolic flux of the 22 reactions of the CCM pathways (including EMP pathway, pentose phosphate (PP) pathway, TCA-cycle, PDH, PDC, and PYC reaction, Fig. 1*A*) as enzymes of these reactions play central roles in controlling the shifting between respiratory and respiro-fermentative metabolic state (15, 21). Then, a kinetic model was proposed to integrate quantitative omics data, including intracellular metabolome, proteome, phosphoproteome, and fluxome data. Subsequently, the Bayesian inference approach (1, 6) combined with the Watanabe–Akaike information criterion (WAIC) was used to infer plausible allosteric effectors (22). Finally, hierarchical regulation (17) and phosphorylation regulation analyses (19) were conducted to determine how allosteric effectors, protein phosphorylation levels, and protein abundance regulated flux changes. The results revealed pathway and metabolism-specific regulatory patterns for *S. cerevisiae*, and the findings provided insight into how fluxes through the CCM are regulated.

Results

Characterizing Flux Differences in *S. cerevisiae* between Respiratory and Respiro-Fermentative Conditions. To decipher flux differences in *S. cerevisiae* between respiratory and respiro-fermentative conditions, we conducted chemostat experiments under nine different specific growth rates (μ = 0.027 h^{-1}, 0.051 h^{-1}, 0.118 h^{-1}, 0.154 h^{-1}, 0.207 h^{-1}, 0.249 h^{-1}, 0.316 h^{-1}, 0.355 h^{-1}, 0.385 h^{-1}) described previously (10). Subsequently, metabolic fluxes (*SI Appendix*, Fig. S1 and Table S6) were quantified using ^{13}C metabolic flux analysis (23). Using the determined absolute flux values, we normalized the flux through an enzyme-catalyzed reaction under different growth rates to that at μ = 0.027 h^{-1} (*SI Appendix*, Table S12). These data mapped the characteristic behavior of metabolic fluxes of different pathways (Fig. 1*B*). Compared with pure respiration, the normalized flux through the EMP pathway increased sharply with the specific growth rates under respiro-fermentation, whereas the normalized flux through the TCA cycle decreased with the specific growth rates. These findings are consistent with an earlier study using the same yeast strain (24). In addition, the normalized flux through the PP pathway linearly increased with the specific growth rates for both respiratory and respiro-fermentative metabolism conditions, indicative of a linear increase in reduced nicotinamide adenine dinucleotide phosphate (NADPH) and precursor demand with increasing specific growth rates.

Enzyme Abundance and Thermodynamic Potential Barely Explain Metabolic Flux Changes in CCM. With the dramatic difference in flux between the respiratory and respiro-fermentative metabolism states, we first explored whether this was associated with enzyme abundance or thermodynamic potential. We therefore calculated the regulation coefficients of protein abundance (ρ_e) and thermodynamic potential ($\rho_{\Delta G}$) using hierarchical regulation analysis for each of the 22 reactions (*SI Appendix*, Tables S13 and S14) for 36 different transitions between specific growth rates. With data from nine specific growth rates, this enabled 15 transitions between respiratory conditions with different specific growth rates, 18 transitions between respiratory and respiro-fermentative conditions, and three transitions between respiro-fermentative conditions with different specific growth rates. Based on the available data, ρ_e and $\rho_{\Delta G}$ were calculated for reactions in the EMP pathway (including the PDC reaction), the PP pathway, and the TCA cycle (including PDH and PYC reaction), as well as for all the three pathways (Fig. 2*A*). For the regulation coefficient of enzyme abundance, it was possible to calculate values for all combinations of reaction flux (22 in total) and conditions (36 in total), i.e., 792 values. In contrast, for $\rho_{\Delta G}$, we only had data on metabolites for calculating 648 values. According to the distributions of ρ_e and $\rho_{\Delta G}$, the proportion of flux changes for reactions across all transitions caused by protein abundance ($0.5 < \rho_e < 2$) or by thermodynamic potential ($0.5 < \rho_{\Delta G} < 2$) could be quantified (Fig. 2*A* and *SI Appendix*, Tables S13–S15). Within these boundaries, protein abundance and thermodynamic potential could explain only about 12% of the flux changes (Fig. 2*A* and *SI Appendix*, Table S15), with protein abundance contributing 14%, whereas thermodynamic potential was responsible for only about 6% (Fig. 2*A* and *SI Appendix*, Tables S13 and S14). The results were consistent with previous reports showing that protein abundance and thermodynamic potential cannot explain flux changes in the CCM (5, 12).

Although protein abundance and thermodynamic potential generally contribute little to flux changes in the whole CCM point of view, dramatic differences of their contribution to flux changes of individual pathway were observed (Fig. 2*B* and *SI Appendix*, Table S13). For example, few fluxes in the EMP (4%) and PP pathways (12%) were controlled by protein abundance across some transitions. In contrast, in the TCA cycle, protein abundance contributed to about 26% of flux changes (Fig. 2*B* and *SI Appendix*, Table S13), demonstrating that the influence of protein abundance regulatory mechanisms was pathway specific. Further analysis showed that flux changes explained by protein abundance for the TCA cycle gradually increased when shifting from respiratory to respiro-fermentative conditions (Fig. 2*B* and *SI Appendix*, Table S13). In addition, we also found that most of the enzymes (17 over 20) showed a high correlation between their abundance and the flux through the reaction they catalyzed (Spearman's correlation coefficient = 1 and $P < 0.05$, *SI Appendix*, Fig. S5 and Table S19). Previous studies showed that repression of the TCA cycle's enzyme-coding gene by extra glucose plays a crucial role in regulating the flux through the pathway (16, 25), and our work confirmed that protein abundance played a key role. Even so, less than half of the flux changes for the TCA cycle under respiro-fermentative conditions were contributed by protein abundance, implying that other factors, such as posttranslational modification of enzymes, reaction product inhibition, or allosteric regulation, may play essential roles in metabolic flux regulation (26).

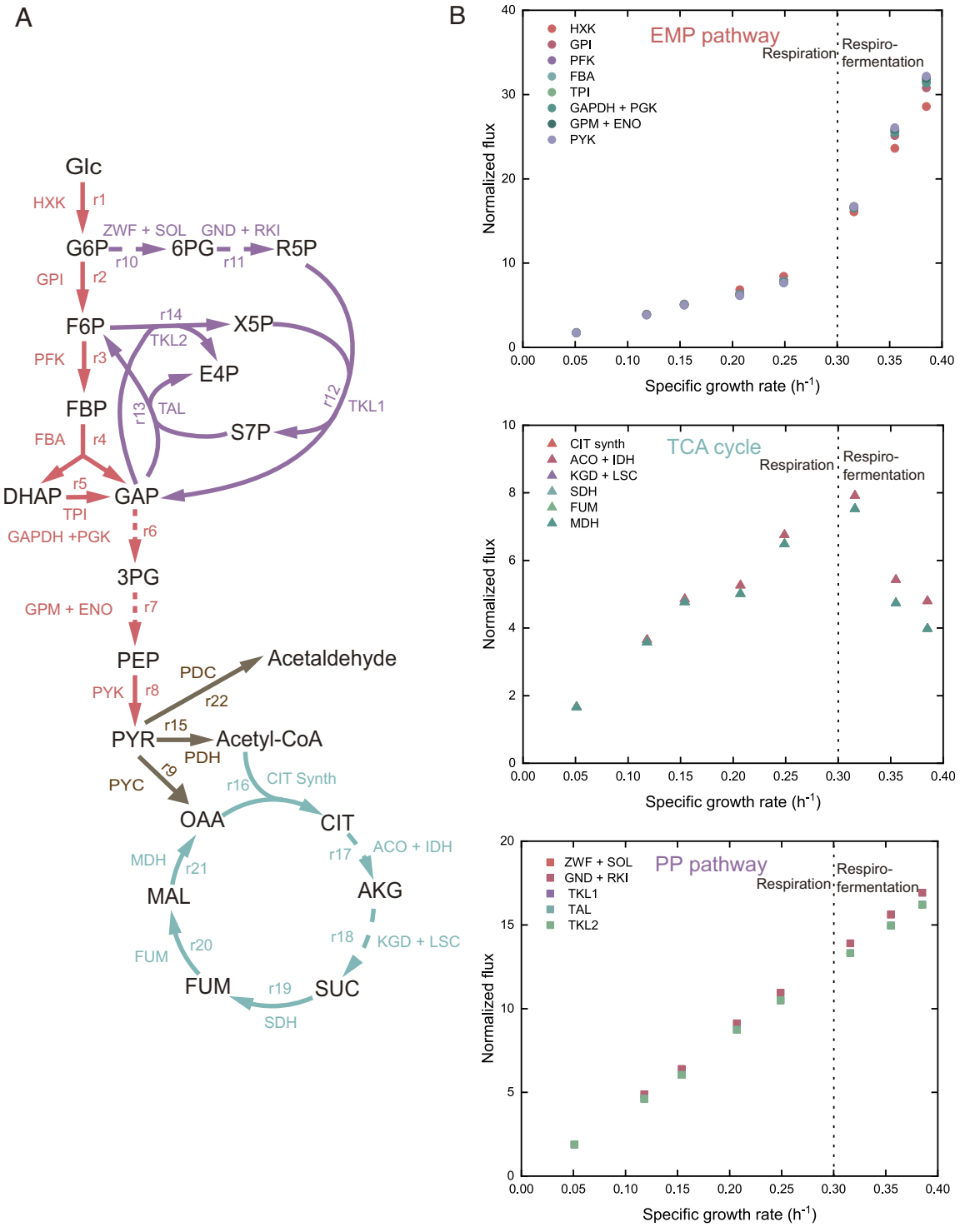

Fig. 1. Metabolic flux for 22 reactions of the CCM altered with specific growth rates. (*A*) Schematic representation of 22 reactions. The dashed line indicates that partial reactions are aggregated into one reaction as the intermediate metabolite of these reactions is not quantified. Different colors of line and font represent different metabolic pathways: red represents the EMP pathway, blue represents the TCA cycle pathway, purple represents the oxidative/nonoxidative pentose phosphate (PP) pathway, and brown represents the other pathways. The black font is the metabolite, whereas the others show the reaction ID and reaction name. (*B*) Flux for each reaction belonging to the EMP pathway (*Upper Left*), TCA cycle (*Upper Right*), and PP pathway (*Lower Left*) altered with specific growth rates. Fluxes under different specific growth rates were normalized to the corresponding flux at $\mu = 0.027\ h^{-1}$. The vertical dotted line indicates the critical specific growth rate, which separates respiration and respiro-fermentation. Abbreviation: Glc: D-glucose; G6P: D-glucose 6-phosphate; F6P: D-fructose 6-phosphate; FBP: D-fructose 1,6-bisphosphate; DHAP: dihydroxyacetone phosphate; GAP: glyceraldehyde 3-phosphate; 3PG: 3-phosphoglycerate; PEP: phosphoenolpyruvate; PYR: pyruvate; CIT: citrate; AKG: 2-oxoglutarate; SUC: succinate; FUM: fumarate; MAL: malate; OAA: oxaloacetate; 6PG: 6-phospho-D-gluconate; R5P: ribose-5-phosphate; X5P: D-xylulose 5-phosphate; E4P: D-erythrose 4-phosphate; S7P: sedoheptulose 7-phosphate; HXK: Hexokinase; GPI, Glucose-6-phosphate isomerase; PFK, Phosphofructokinase; FBA, Fructose-bisphosphate aldolase; TPI, Triose-phosphate isomerase; GAPDH + PGK: glyceraldehyde-3-phosphate dehydrogenase + phosphoglycerate kinase; GPM + ENO: phosphoglycerate mutase + enolase; PYK: Pyruvate kinase; PYC: Pyruvate carboxylase; ZWF + SOL: Glucose 6-phosphate dehydrogenase + 6-phosphogluconolactonase; GND + RKI: phosphogluconate dehydrogenase + ribose-5-phosphate isomerase; TKL1: Transketolase 1; TAL: Transaldolase1; TKL2: Transketolase 2; PDH: Pyruvate dehydrogenase; CIT Synth: Citrate synthase; ACO + IDH: citrate to cis-aconitate + cis-aconitate to isocitrate+ isocitrate dehydrogenase; KGD + LSC: oxoglutarate dehydrogenase + succinate-CoA ligase; SDH: succinate dehydrogenase; FUM: Fumarase; MDH: Malate dehydrogenase; PDC: Pyruvate decarboxylase.

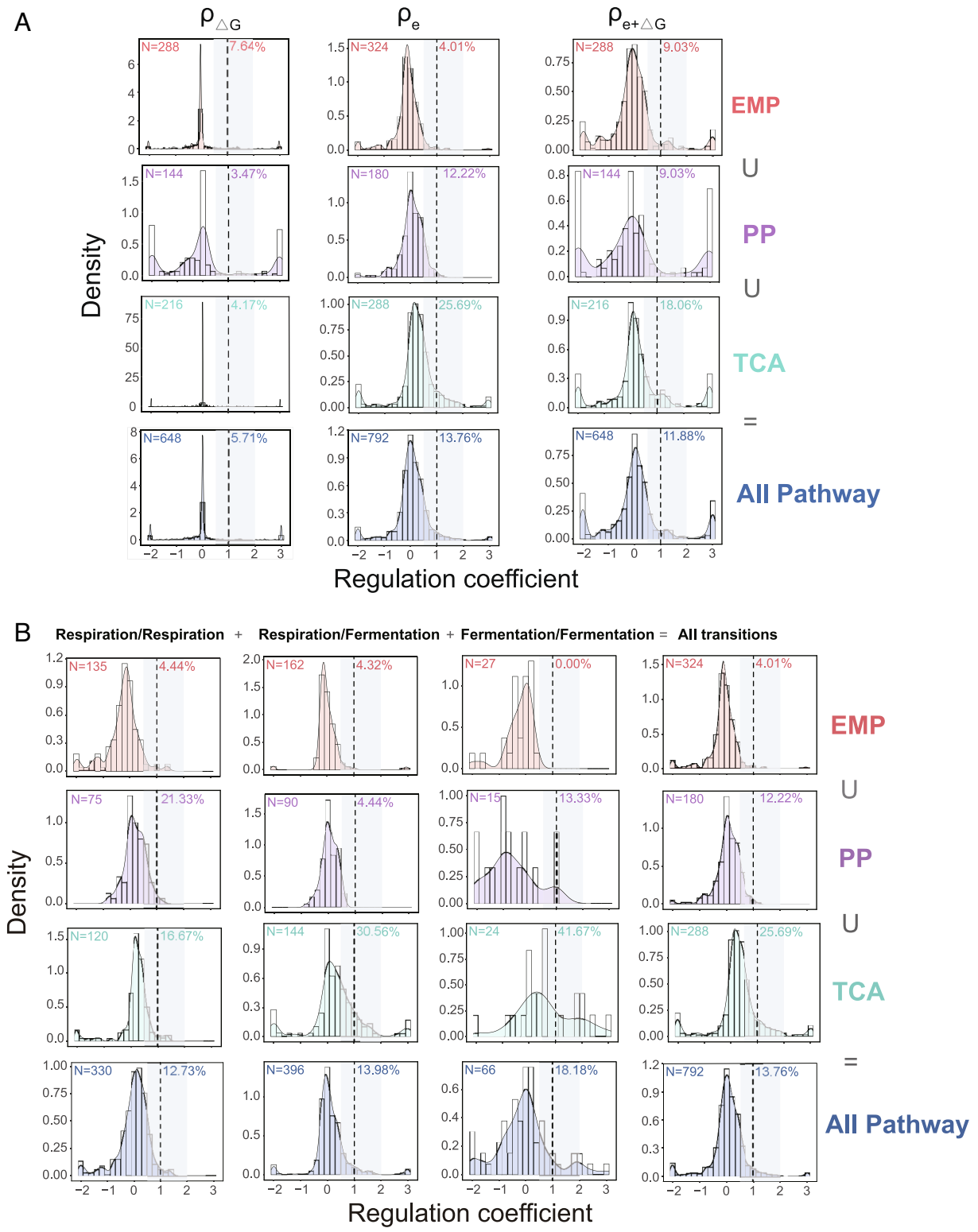

Fig. 2. Distributions of coefficients for thermodynamic potential ($\rho_{\Delta G}$) and protein abundance (ρ_e) regulation of fluxes. (*A*) Distribution of coefficients for protein abundance plus thermodynamic potential ($\rho_{e+\Delta G}$), thermodynamic potential ($\rho_{\Delta G}$), and protein abundance (ρ_e) regulation. The number of flux changes considered for each factor is in the upper left corner (N). The percentages in each plot quantify the fraction of flux changes explained by the corresponding factors ($0.5 < \rho < 2$, gray interval). Different colors represent different metabolic pathways. (*B*) Distributions of regulation coefficients for protein abundance (ρ_e) under different pathways and regimes. Respiration/Respiration means both pairs of transitions included respiratory metabolism. Fermentation/Fermentation means both pairs of transitions included respiro-fermentative metabolism. Respiration/Fermentation means pairs of transitions between respiratory and respiro-fermentative metabolism. EMP, Embden–Meyerhof–Parnas pathway; PP, pentose phosphate pathway; TCA, tricarboxylic acid cycle.

Allosteric Regulation Exert Significant Flux Control of the EMP and PP Pathways under Respiratory Conditions. Next, we evaluated whether flux changes were associated with changes in the concentrations of substrates and allosteric effectors (hereafter collectively referred to as metabolite concentrations). We constructed a nonlinear kinetic model in which enzyme

abundance, substrate concentration, thermodynamic potential, and concentration of putative allosteric effectors were included to infer plausible allosteric effectors based on Bayesian inference (1, 6, 12, 27). Details are provided in the "Bayesian inference for plausible allosteric effectors" and "Details of Bayesian inference plausible allosteric effectors and results analysis" sections in *SI Appendix*. Using the kinetic model, the regulation coefficient of metabolites (ρ_m) was calculated based on hierarchical regulation analysis to determine the proportion of functional regulatory events caused by metabolite concentration ($0.5 < \rho_m < 2$).

Each of the 54 putative allosteric effectors from the BRaunschweig ENzyme DAtabase (BRENDA) database of the 22 reactions was assessed by the Bayesian approach to identify plausible effectors. Among these in vitro effectors, six showed an in vivo metabolic regulation function previously (6, 21, 28–33). To estimate pointwise out-of-sample prediction accuracy from a fitted Bayesian model, we employed the WAIC (22). WAIC is based on the series expansion of leave-one-out cross-validation, and higher WAIC with a newly added effector to the model means better fitting of the model (34). Our analysis identified six reactions for which their fluxes were significantly controlled by allosteric effectors, with one reaction controlled by two effectors, meaning that a total of seven effectors were identified (Fig. 3 and *SI Appendix*, Table S8). An illustrative example is the phosphofructokinase (PFK) reaction in the EMP pathway, for which we tested five putative effectors (*SI Appendix*, Fig. S3 and Table S7). Among these effectors, our approach found that adenosine triphosphate and adenosine diphosphate showed cooperative regulation (the highest WAIC), while others were not supported (lower WAIC than strongly supported effectors, *SI Appendix*, Fig. S3 and Table S7). However, three of these effectors supported by our approach have been reported to show an in vivo metabolic regulation function, only accounting for 50% (three over six). This result shows that not all the effectors having an in vivo function can be identified by our Bayesian approach. For example, citrate was previously reported as an inhibitor of the pyruvate kinase isozyme (Cdc19) (6) but was not inferred to be an inhibitor in this study (lower WAIC than strongly supported effectors; *SI Appendix*, Table S7). However, this may be due to differences in culture conditions since Hackett et al. (2016) used nitrogen- and leucine-limited chemostats (6), whereas we used glucose-limited chemostats. Moreover, all these supported effectors were highly enriched for in vivo functional regulatory interactions (based on Fisher's exact test, $P < 0.05$, *SI Appendix*, Table S9), validating this approach. Furthermore, all supported effectors identified by our approach have been verified by biochemical experiments in vitro. Both statistical and experimental evidence indicated that allosteric effectors identified by our approach most likely take function under different specific growth rates.

Next, the proportion of functional regulatory events influenced by metabolite concentration was determined for all ρ_m values. According to the criterion ($0.5 < \rho_m < 2$), about 19% of flux changes in the CCM were due to changes in metabolite concentrations (Fig. 4 and *SI Appendix*, Table S16). A similar proportion was also found for *Escherichia coli* cultured in chemostats (12), showing that metabolite concentrations do not fully explain flux changes within the CCM. However, the contribution for flux control exerted by metabolites varied among the three pathways in the CCM. Thus, flux changes for the TCA cycle explained by changes in metabolite concentrations were only about 6%, whereas it was higher for both the EMP (17.9%) and PP (41.7%) pathways (Fig. 4 and *SI Appendix*, Table S16). Consistently, no allosteric effectors were identified for the TCA cycle (Fig. *3*).

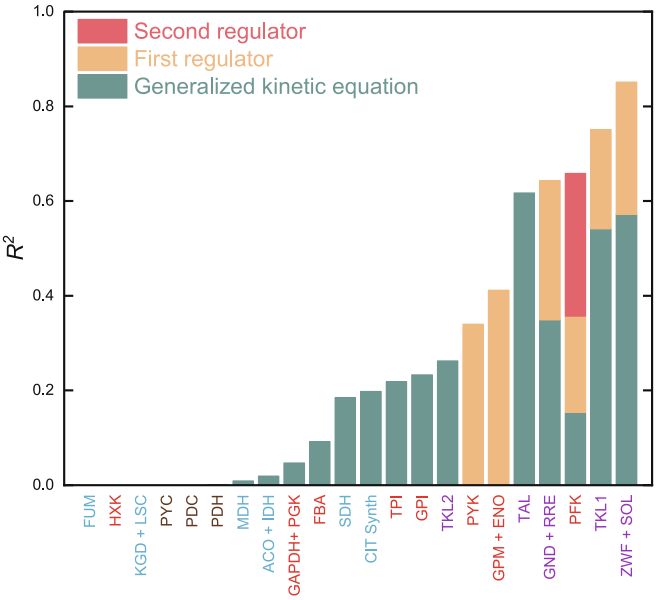

Fig. 3. Linear fitting results between observed flux and flux predicted by the kinetic model for 22 reactions in the CCM of budding yeast. R^2 is the coefficient determined through linear fitting between the observed flux and the output of the kinetic model predicted under nine dilution rates (R^2 was considered zero when the slope of linear fitting was negative). Green bars are the fitting results between the generalized kinetic model (without any allosteric effectors) and the observed flux, while yellow and red bars are the fitting results between the observed flux and the kinetic model with one (first allosteric effector) or two (second allosteric effector) plausible allosteric effectors inferred by Bayesian inference. Different colors of reaction names represent different metabolic pathways; purple represents the PP pathway, red represents the EMP pathway, blue represents the TCA cycle, and brown represents other pathways. HXK: Hexokinase; GPI, Glucose-6-phosphate isomerase; PFK, Phosphofructokinase; FBA, Fructose-bisphosphate aldolase; TPI, Triose-phosphate isomerase; GAPDH + PGK: glyceraldehyde-3-phosphate dehydrogenase + phosphoglycerate kinase; GPM + ENO: phosphoglycerate mutase + enolase; PYK: Pyruvate kinase; PYC: Pyruvate carboxylase; ZWF + SOL: Glucose 6-phosphate dehydrogenase + 6-phosphogluconolactonase; GND + RKI: phosphogluconate dehydrogenase + ribose-5-phosphate isomerase; TKL1: Transketolase 1; TAL: Transaldolase1; TKL2: Transketolase 2; PDH: Pyruvate dehydrogenase; CIT Synth: Citrate synthase; ACO + IDH: citrate to cis-aconitate (3-) + cis-aconitate (3-) to isocitrate+ isocitrate dehydrogenase; KGD + LSC: oxoglutarate dehydrogenase + succinate-CoA ligase; SDH: succinate dehydrogenase; FUM: Fumarase; MDH: Malate dehydrogenase; PDC: Pyruvate decarboxylase.

Furthermore, flux changes explained by metabolic concentrations for the EMP pathway were much higher under respiratory conditions (20.7%) than those under respiro-fermentative conditions (3.7%), indicating that metabolites had a more significant impact on glycolytic flux under purely respiratory conditions. This can of course also have been an effect of lower specific growth rates. A similar observation was also found for the PP pathway, except that almost no flux changes can be explained by metabolite concentrations under respiro-fermentative conditions (Fig. 4 and *SI Appendix*, Table S16).

Our analysis indicates that flux regulation by metabolite concentration was more predominant under pure respiratory than under respiro-fermentative conditions. To explain this phenomenon, absolute concentrations of these inferred plausible allosteric effectors under respiratory and respiro-fermentative conditions were compared. Two allosteric effectors showed statistically significant differences between the two metabolic conditions (*SI Appendix*, Fig S4 and Table S17). Thus, the concentrations of 3-phosphoglycerate (an inferred and actual inhibitor of phosphoglycerate mutase) and phosphoenolpyruvate (an inferred and actual inhibitor of glucose 6-phosphate dehydrogenase and

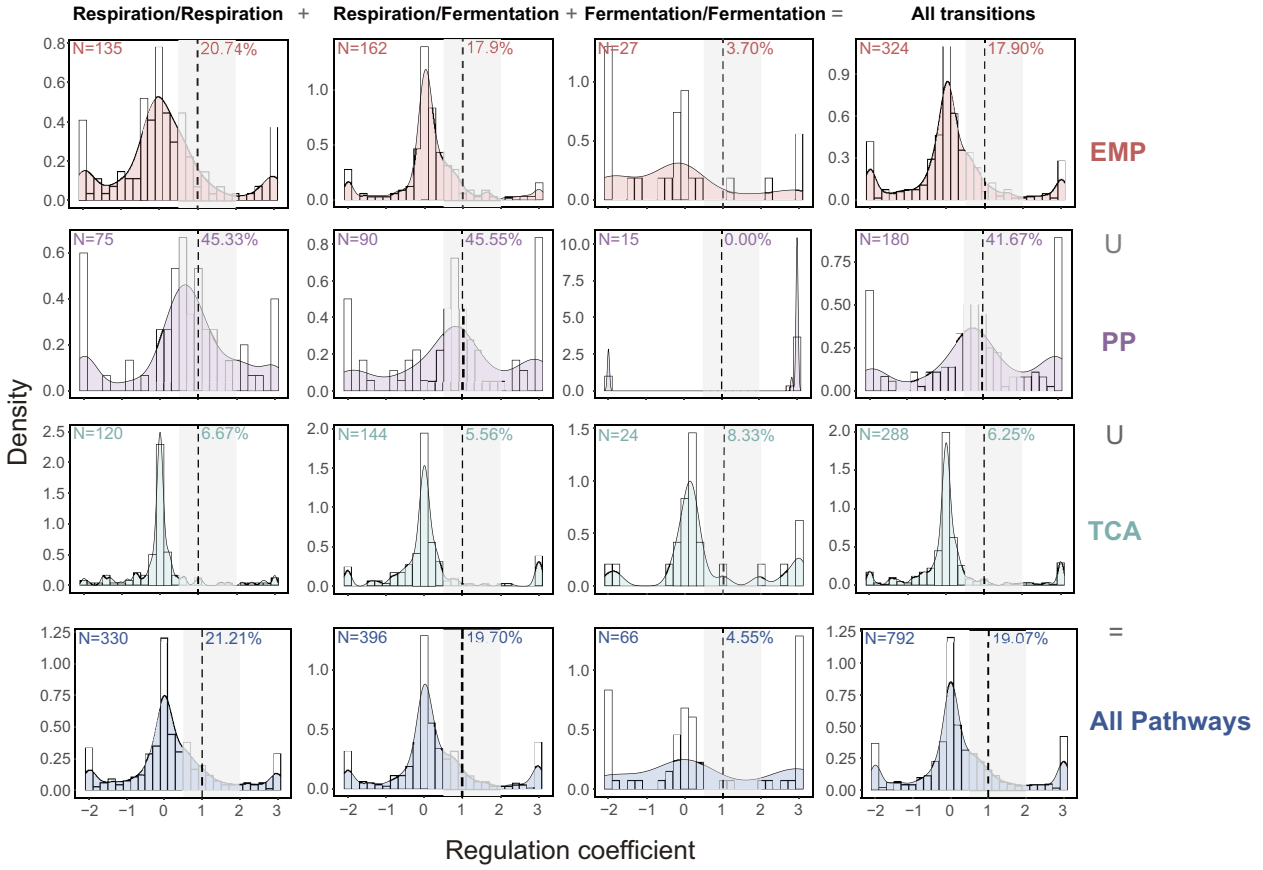

Fig. 4. Distributions of coefficients for metabolic concentration regulation (ρ_m). The number of flux changes considered for each pathway is given in the upper left corner (N). The percentages in each plot quantify the fraction of flux changes explained by the corresponding mechanism ($0.5 < \rho_m < 2$, gray interval). Different colors represent different metabolic pathways. Respiration/Respiration means both pairs of transitions were at respirative metabolism. Fermentation/Fermentation means both pairs were at respiro-fermentative metabolism. Respiration/Fermentation means pairs of transitions between respirative and respiro-fermentative metabolism. EMP, Embden–Meyerhof–Parnas pathway; PP, pentose phosphate pathway; TCA, tricarboxylic acid cycle.

transketolase 1) were significantly higher under purely respiration conditions (*t* test with $P < 0.05$, *SI Appendix*, Fig. S4). This difference in absolute concentrations between the two metabolic conditions may explain the larger number of functional regulatory events caused by metabolite concentration under respiratory conditions than under respiro-fermentative conditions, because the corresponding allosteric effectors only take function under purely respiratory conditions. This phenomenon was relevant for both the EMP and PP pathways.

Protein Phosphorylation Influences EMP Pathway Flux Changes, Especially under Respiratory Conditions. Next, we evaluated the overall contribution (ρ_{er}) to the flux regulation given by the sum of the individual regulation coefficients considered in this work ($\rho_{er} = \rho_e + \rho_{\Delta G} + \rho_m$). Together, they covered about 30% of flux regulation in the EMP pathway, about 36% in the TCA cycle, and about 57% in the PP pathway (Figs. 2*A* and 4). Therefore, other flux regulatory factors we did not consider in this work should be functional, and here we evaluated flux changes explained by enzyme phosphorylation levels using phosphorylation regulation analysis (19). Phosphorylation data were obtained from our previously published study (four of the nine dilution rates included phosphorylation data: 0.027 h^{-1}, 0.154 h^{-1}, 0.355 h^{-1}, and 0.385 h^{-1}) (10). Enzyme phosphorylation regulation is pathway specific. Among all CCM pathways, events that link to enzyme phosphorylation which regulates the activity of the metabolic enzymes (hereafter referred to as functional phosphorylation events) were more predominant for the EMP pathway than for the other two pathways (Fig. 5 and *SI Appendix*, Table S18), which is consistent with earlier findings (35).

To evaluate how protein phosphorylation contributes to flux regulation between respiratory and respiro-fermentative conditions, we calculated the fraction of functional phosphorylation events among all phosphorylation events. And dramatic differences were found between respiratory and respiro-fermentative conditions (Fig. 5 and *SI Appendix*, Table S18). Functional phosphorylation events were more predominant under respiratory conditions (69%) than those during the shift from respiratory to respiro-fermentative conditions (34%). At respiro-fermentative conditions, about 38% of the phosphorylation events were functional. Furthermore, we noticed that most functional phosphorylation events (21 over 22) under respiratory conditions were more likely to be inferred as inhibitory phosphorylation events. However, only 28 over 42 (66.7%) functional phosphorylation events were inferred to be inhibitory under shifting from respiratory to respiro-fermentative conditions, whereas it decreased to 5 over 11 (45.5%) under respiro-fermentative conditions. These results showed that inhibitory phosphorylation event proportion seems to prevail under respiratory conditions than under respiro-fermentative conditions. Moreover, this phenomenon may imply that different functional phosphorylation events played different roles under different conditions, mainly inhibitory events under respiratory conditions and activated events under respiro-fermentative conditions, supporting a rapid increase in glycolytic flux to meet ever-increasing growth rates. Even so, these results did not demonstrate that the flux changes through the EMP

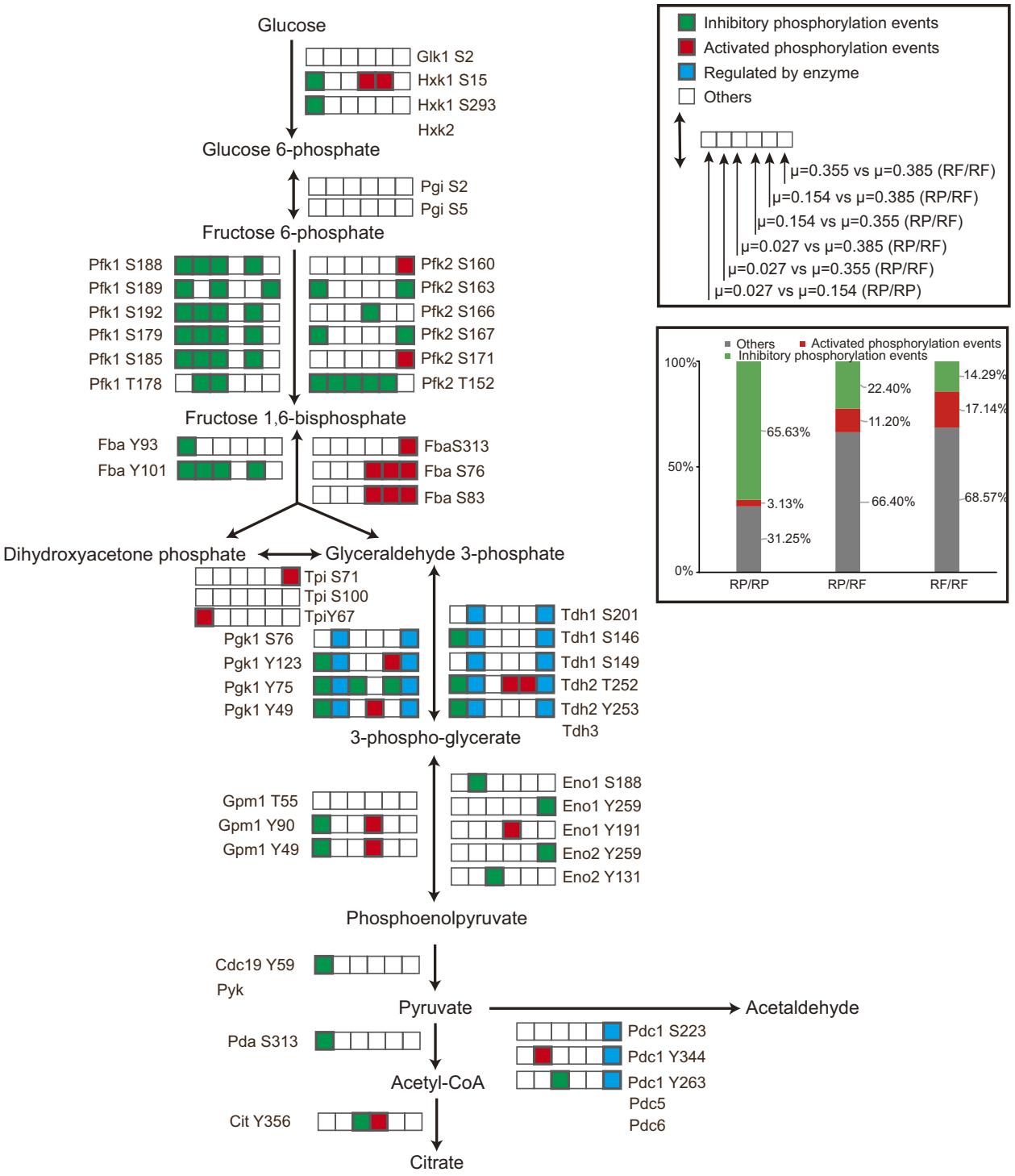

Fig. 5. Phosphorylation regulation analysis mapped onto glycolysis in budding yeast. Six transitions were constructed under four different dilution rates (μ = 0.027 h^{-1}, 0.154 h^{-1}, 0.355 h^{-1}, 0.385 h^{-1}). RP/RF means transitions between respiratory and respiro-fermentative metabolism (0.027 h^{-1} vs. 0.355 h^{-1}, 0.027 h^{-1} vs. 0.385 h^{-1}, 0.154 h^{-1} vs. 0.355 h^{-1}, 0.154 h^{-1} vs. 0.385 h^{-1}). RP/RP means both transitions were within respiratory metabolism (0.051 h^{-1} vs. 0.154 h^{-1}). RF/RF means both pairs of transitions were within respiro-fermentative metabolism (0.355 h^{-1} vs. 0.385 h^{-1}). GLK1 S2 means the second amino acid of glucokinase, a serine, is phosphorylated under glucose-limiting chemostats, and enzymes are marked similarly. The proportions of inhibitory and activated phosphorylation events among all phosphorylation events under different transitions are shown on the right. Abbreviation: Glk, glucokinase; Hxk, hexokinase; Pgi, glucose-6-phosphate isomerase; Pfk, phosphofructokinase; Fba, fructose 1,6-bisphosphate aldolase; Tpi, triose phosphate isomerase; Tdh, glyceraldehyde-3-phosphate dehydrogenase; Pgk, 3-phosphoglycerate kinase; Eno, enolase; Gpm, phosphoglycerate mutase; Cdc19 and Pyk, pyruvate kinase; Pda, pyruvate dehydrogenase; Cit, citrate synthase; Pdc, pyruvate decarboxylase.

pathway contributed by enzyme phosphorylation levels are predominant, as the functional phosphorylation events' proportion is about 40% to all the phosphorylation events (*SI Appendix*, Table S18), indicating that other unknown regulatory factors also play a central role in flux regulation.

Discussion

Here, we performed a detailed analysis of how flux through 22 key reactions in the CCM of *S. cerevisiae* is controlled under glucose-limited chemostats at nine different dilution rates. Proteomics data

were used to quantify flux regulation by protein abundance, whereas metabolomics data were used to evaluate the thermodynamic potential effect. To evaluate metabolite regulation, we constructed a kinetic model to quantify flux regulation by metabolite concentration, including allosteric regulation. By comparing the proportions of functional regulatory events caused by different regulatory factors, our results revealed that flux changes were controlled by coordinating different regulatory factors. Enzyme abundance and thermodynamic potential exert only a low-level regulation of metabolic flux changes in the CCM. Similar findings were reported in *E. coli* and *Bacillus subtilis* (5, 12). However, flux changes explained by metabolite concentration were more prevalent than those explained by enzyme abundance and thermodynamic potential.

Our results also revealed that some regulatory factors were more dominant for specific reactions. Thus, flux changes explained by enzyme abundance in the TCA cycle were more dominant than those in the EMP and PP pathways. In contrast, flux changes contributed by metabolite concentration and protein phosphorylation displayed the opposite trend. This pathway-specific regulation pattern was also found in *E. coli* under different chemostat conditions (12). Moreover, this regulatory pattern appears essential in response to specific conditions (36). Compared with the respiratory metabolism state, genes involved in the oxidative phosphorylation pathway are repressed at high specific growth rates (respiro-fermentative condition), and the translation efficiency of the ribosome is lowered under respiro-fermentative conditions for *S. cerevisiae* (16, 37). These controls inevitably led to lower mitochondrial protein levels and a stronger correlation between protein concentration and metabolic flux. In contrast, metabolite concentrations and protein phosphorylation levels were correlated more strongly with metabolic fluxes in the EMP and PP pathways because most plausible allosteric effectors and functional phosphorylation sites were identified in these pathways (10, 38). However, more peripheral parts of metabolism, i.e., outside CCM pathways, might have simpler control mechanisms. For example, flux changes seem tightly intertwined with enzyme abundance in cell signaling and metabolism-regulating transcriptional networks. One reason is that abundance changes evolve much easier than allosteric mechanisms. Another reason is the higher cost of regulating flux using a small molecule effector (39, 40).

Another interesting finding is that increasing glycolytic flux along with specific growth rate was accompanied by decreased flux changes contributed by metabolite concentration and enzyme phosphorylation level. Further investigation of allosteric effectors showed that the concentration of allosteric inhibitors under respiratory conditions was significantly higher than that under respiro-fermentative conditions. This phenomenon is consistent with previous reports showing that metabolite concentration is altered first, and V_{max} is altered later during transitions from low glucose aerobic conditions to high glucose anaerobic respiration in *S. cerevisiae* (30). However, why *S. cerevisiae* regulates EMP pathway flux and enzyme activity in this way remains unclear. We assumed that yeast cells had evolved corresponding mechanisms to allocate their resources to quickly adapt to fluctuations (such as circadian temperature) and thereby adapt to changes in nutrient availability in their natural habitat (41, 42). It is also reported that *S. cerevisiae* allocates more glycolytic enzymes than are needed under low glucose concentrations (10), primed and ready if a sudden increase in the availability of extracellular glucose should occur (43).

However, about 65% of metabolic flux changes could not be explained by metabolite concentration, thermodynamic potential, or enzyme abundance. One reason is that phosphorylation regulation plays a vital role in regulating flux changes (19, 35). Though it was impossible to quantify the ratio of functional phosphorylation events, as a protein possesses many phosphorylation sites, our analysis showed that protein phosphorylation levels were most strongly associated with pathway flux regulation in the EMP compared with the TCA cycle or the PP pathway. However, this result did not demonstrate that the flux changes through the EMP pathway contributed by the phosphorylation level changes are predominant as the functional phosphorylation events' proportion is less than 40% when considering all the phosphorylation events. Another possible reason is that our kinetic model is too simple to miss some complex interactions in vivo. For example, previously reported allosteric effectors whose function are verified in vivo, such as adenosine monophosphate (an activator of PFK) (33) and NADPH (an inhibitor of glucose 6-phosphate dehydrogenase) (21, 32), were rejected by our model. Moreover, our model did not consider the effects of changes in enzyme abundance of a reaction on flux changes through other reactions belonging to the same pathways. These complex interactions can be further quantified by metabolic control analysis (1, 6, 44). The third reason is that other regulatory factors (e.g., posttranscription and other posttranslation regulation factors) not considered in this work may play a role in flux control.

Hierarchical regulation analysis is a classical formalism that can quantify the relative contribution of individual regulatory factors to regulating the flux. Previous reports used this method to quantify the flux changes contributed by transcription, translation, protein degradation, protein abundance, thermodynamics potential, and substrate concentrations (12, 13). However, flux changes contributed by allosteric concentrations and phosphorylation levels have not been quantified. The major challenge is establishing methods to identify allosteric effectors and phosphorylation events that function in vivo under specific conditions. Fortunately, Hackett et al. (2016) developed a method for identifying plausible allosteric effectors through a Michaelis–Menten equation using Bayesian inference (6). In addition, Chen et al. (2017) also introduced a way capable of identifying functional phosphorylation events (19). Based on their work, we finally quantified the flux changes contributed by allosteric effector concentration and phosphorylation levels in this study. Except for phosphorylation regulation, this method can also be extended to quantify the contribution of other posttranslational modifications, such as acetylation and succinylation, to metabolic reaction flux changes in any organisms. However, this method has some limitations. For example, the constructed kinetic model rejected some allosteric effectors which take a function in vivo due to either measurement error, unmeasured omics data, or subcellular localization caused by compartmentation. Therefore, a more complex kinetic model, deeper omics data coverage, and more accurate assessment of functional phosphorylation events will advance further studies on hierarchical regulation analysis. Moreover, extending the study conditions to genetic perturbations (e.g., gene knockout) makes it possible to investigate on a larger scale, thereby making the results more reliable.

In conclusion, our results revealed pathway-specific, metabolic state–specific, and multilevel regulation mechanisms in *S. cerevisiae.* Glycolytic flux increased with specific growth rates, and this increase was driven by a decrease in flux changes explained by altered metabolite concentrations (allosteric inhibitors) and altered functional phosphorylation events (mainly a decrease in phosphorylation level). Although further investigation is needed to decipher the underlying principles of these regulatory mechanisms, our study provides valuable insight into fundamental metabolic regulation patterns in yeast CCM under different glucose-limited chemostats. The findings will help to identify regulatory mechanisms in yeast.

Materials and Methods

All of the materials and methods are detailed in *SI Appendix*: strains and media; culture conditions; data acquisition; quantification of extracellular metabolites; quantification of intracellular metabolites; MDV (Mass Distribution Vector) measurements; determination of specific rates; metabolic flux estimation; proteome and phosphorylation proteome; estimation of thermodynamic potentials; Bayesian inference for plausible allosteric effectors; details of Bayesian inference plausible allosteric effector and result analysis; estimation of regulation coefficients; phosphorylation regulation analysis. Code to apply the Bayesian approach to infer plausible allosteric effectors is available on GitHub (https://github.com/chenmin531/Hierachical-regulation-analysis.git).

Data, Materials, and Software Availability. Proteomics data have been deposited in ProteomeXchange's Proteomics Identification Database Archive Metabolites raw data was uploaded to MetaboLights (PXD012891 MTBLS6444) (45, 46).

ACKNOWLEDGMENTS. We thank Peng Liu for supplying ^{13}C internal standards and Jiaqi Wang for experimental assistance and collecting omics samples. We thank International Science Editing (http://www.internationalscienceediting.com) for editing this manuscript. This work was financially supported by the National Natural Science Foundation of China (No. 21776082) and the Knut and Alice Wallenberg Foundation.

Author affiliations: [a]State Key Laboratory of Bioreactor Engineering, East China University of Science and Technology, Shanghai 200237, China; [b]Key Laboratory of Engineering Biology for Low-Carbon Manufacturing, Tianjin Institute of Industrial Biotechnology, Chinese Academy of Sciences, Tianjin 300308, China; [c]Department of Biology and Biological Engineering, Chalmers University of Technology, Gothenburg SE41296, Sweden; and [d]BioInnovation Institute, DK2200 Copenhagen N, Denmark

Author contributions: J.X. and J.N. designed research; M.C., T.X., H.L., Y.Z., and J.X. performed research and analyzed data; and M.C., J.X. and J.N. wrote the paper.

Reviewers: J.T.P., Technische Universiteit Delft; and M.R., Charite – Universitatsmedizin Berlin Institut fur Medizin-Pflegepadagogik und Pflegewissenschaft.

1. P. C. St John, J. Strutz, L. J. Broadbelt, K. E. J. Tyo, Y. J. Bomble, Bayesian inference of metabolic kinetics from genome-scale multiomics data. *PLoS Comput. Biol.* **15**, e1007424 (2019).
2. J. Nielsen, J. D. Keasling, Engineering cellular metabolism. *Cell* **164**, 1185–1197 (2016).
3. P. C. St John, Y. J. Bomble, Approaches to computational strain design in the multiomics era. *Front. Microbiol.* **10**, 597 (2019).
4. P. Daran-Lapujade *et al.*, The fluxes through glycolytic enzymes in Saccharomyces cerevisiae are predominantly regulated at posttranscriptional levels. *Proc. Natl. Acad. Sci. U.S.A.* **104**, 15753–15758 (2007).
5. V. Chubukov *et al.*, Transcriptional regulation is insufficient to explain substrate-induced flux changes in Bacillus subtilis. *Mol. Syst. Biol.* **9**, 709 (2013).
6. S. R. Hackett *et al.*, Systems-level analysis of mechanisms regulating yeast metabolic flux. *Science* **354**, aaf2786 (2016).
7. A. Zelezniak *et al.*, Machine learning predicts the yeast metabolome from the quantitative proteome of kinase knockouts. *Cell Syst.* **7**, 269–283.e266 (2018).
8. M. M. Mihaylova, R. J. Shaw, The AMPK signalling pathway coordinates cell growth, autophagy and metabolism. *Nat. Cell Biol.* **13**, 1016–1023 (2011).
9. A. Gonzalez, M. N. Hall, Nutrient sensing and TOR signaling in yeast and mammals. *EMBO J.* **36**, 397–408 (2017).
10. J. Xia *et al.*, Proteome allocations change linearly with the specific growth rate of Saccharomyces cerevisiae under glucose limitation. *Nat. Commun.* **13**, 2819 (2022).
11. B. H. ter Kuile, H. V. Westerhoff, Transcriptome meets metabolome: Hierarchical and metabolic regulation of the glycolytic pathway. *FEBS Lett.* **500**, 169–171 (2001).
12. L. Gerosa *et al.*, Pseudo-transition analysis identifies the key regulators of dynamic metabolic adaptations from steady-state data. *Cell Syst.* **1**, 270–282 (2015).
13. J. Postmus *et al.*, Quantitative analysis of the high temperature-induced glycolytic flux increase in Saccharomyces cerevisiae reveals dominant metabolic regulation. *J. Biol. Chem.* **283**, 23524–23532 (2008).
14. E. Postma, C. Verduyn, W. A. Scheffers, J. P. Van Dijken, Enzymic analysis of the crabtree effect in glucose-limited chemostat cultures of Saccharomyces cerevisiae. *Appl. Environ. Microbiol.* **55**, 468–477 (1989).
15. J. T. Pronk, H. Yde Steensma, J. P. Van Dijken, Pyruvate metabolism in Saccharomyces cerevisiae. *Yeast* **12**, 1607–1633 (1996).
16. J. M. Gancedo, The early steps of glucose signalling in yeast. *FEMS Microbiol. Rev.* **32**, 673–704 (2008).
17. K. van Eunen, S. Rossell, J. Bouwman, H. V. Westerhoff, B. M. Bakker, Quantitative analysis of flux regulation through hierarchical regulation analysis. *Methods Enzymol.* **500**, 571–595 (2011).
18. A. P. Oliveira, U. Sauer, The importance of post-translational modifications in regulating Saccharomyces cerevisiae metabolism. *FEMS Yeast Res.* **12**, 104–117 (2012).
19. Y. Chen, Y. Wang, J. Nielsen, Systematic inference of functional phosphorylation events in yeast metabolism. *Bioinformatics* **33**, 1995–2001 (2017).
20. I. Piazza *et al.*, A map of protein-metabolite interactions reveals principles of chemical communication. *Cell* **172**, 358–372.e323 (2018).
21. G. G. Zampar *et al.*, Temporal system-level organization of the switch from glycolytic to gluconeogenic operation in yeast. *Mol. Syst. Biol.* **9**, 651 (2013).
22. A. Vehtari, A. Gelman, J. Gabry, Practical Bayesian model evaluation using leave-one-out cross-validation and WAIC. *Stat. Comput.* **27**, 1413–1432 (2017).
23. S. Kajihata, C. Furusawa, F. Matsuda, H. Shimizu, OpenMebius: An open source software for isotopically nonstationary 13C-based metabolic flux analysis. *Biomed. Res. Int.* **2014**, 627014 (2014).
24. C. A. Suarez-Mendez *et al.*, Interaction of storage carbohydrates and other cyclic fluxes with central metabolism: A quantitative approach by non-stationary (13)C metabolic flux analysis. *Metab. Eng. Commun.* **3**, 52–63 (2016).
25. S. Christen, U. Sauer, Intracellular characterization of aerobic glucose metabolism in seven yeast species by 13C flux analysis and metabolomics. *FEMS Yeast. Res.* **11**, 263–272 (2011).
26. Y. Chen, J. Nielsen, Energy metabolism controls phenotypes by protein efficiency and allocation. *Proc. Natl. Acad. Sci. U.S.A.* **116**, 17592–17597 (2019).
27. A. D. McNaughton *et al.*, Bayesian inference for integrating yarrowia lipolytica multiomics datasets with metabolic modeling. *ACS Synth. Biol.* **10**, 2968–2981 (2021).
28. R. A. Poorman, A. Randolph, R. G. Kemp, R. L. Heinrikson, Evolution of phosphofructokinase–gene duplication and creation of new effector sites. *Nature* **309**, 467–469 (1984).
29. H. R. Christofk, M. G. Vander Heiden, N. Wu, J. M. Asara, L. C. Cantley, Pyruvate kinase M2 is a phosphotyrosine-binding protein. *Nature* **452**, 181–U127 (2008).
30. J. van den Brink *et al.*, Dynamics of glycolytic regulation during adaptation of Saccharomyces cerevisiae to fermentative metabolism. *Appl. Environ. Microbiol.* **74**, 5710–5723 (2008).
31. Y. F. Xu *et al.*, Regulation of yeast pyruvate kinase by ultrasensitive allostery independent of phosphorylation. *Mol. Cell* **48**, 52–62 (2012).
32. D. Christodoulou *et al.*, Reserve flux capacity in the pentose phosphate pathway enables Escherichia coli's rapid response to oxidative stress. *Cell Syst.* **6**, 569–578.e567 (2018).
33. D. D. van Niekerk *et al.*, Phosphofructokinase controls the acetaldehyde-induced phase shift in isolated yeast glycolytic oscillators. *Biochem. J.* **476**, 353–363 (2019).
34. J. Salvatier, T. V. Wiecki, C. Fonnesbeck, Probabilistic programming in Python using PyMC3. *PeerJ Comput. Sci.* **2**, e55 (2016).
35. A. P. Oliveira *et al.*, Regulation of yeast central metabolism by enzyme phosphorylation. *Mol. Syst. Biol.* **8**, 623 (2012).
36. N. G. Walter, Biological pathway specificity in the cell-does molecular diversity matter? *Bioessays* **41**, e1800244 (2019).
37. C. Malina, R. Yu, J. Bjorkeroth, E. J. Kerkhoven, J. Nielsen, Adaptations in metabolism and protein translation give rise to the Crabtree effect in yeast. *Proc. Natl. Acad. Sci. U.S.A.* **118**, e2112836118 (2021).
38. N. Hammad, M. Rosas-Lemus, S. Uribe-Carvajal, M. Rigoulet, A. Devin, The Crabtree and Warburg effects: Do metabolite-induced regulations participate in their induction? *Biochim. Biophys. Acta* **1857**, 1139–1146 (2016).
39. M. T. Alam *et al.*, The self-inhibitory nature of metabolic networks and its alleviation through compartmentalization. *Nat. Commun.* **8**, 16018 (2017).
40. E. Reznik *et al.*, Genome-scale architecture of small molecule regulatory networks and the fundamental trade-off between regulation and enzymatic activity. *Cell Rep.* **20**, 2666–2677 (2017).
41. L. A. Cruz *et al.*, Similar temperature dependencies of glycolytic enzymes: An evolutionary adaptation to temperature dynamics? *BMC Syst. Biol.* **6**, 151 (2012).
42. M. Hebly *et al.*, Physiological and transcriptional responses of anaerobic chemostat cultures of Saccharomyces cerevisiae subjected to diurnal temperature cycles. *Appl. Environ. Microbiol.* **80**, 4433–4449 (2014).
43. D. Davidi, L. M. Longo, J. Jablonska, R. Milo, D. S. Tawfik, A bird's-eye view of enzyme evolution: Chemical, physicochemical, and physiological considerations. *Chem. Rev.* **118**, 8786–8797 (2018).
44. P. Millard, K. Smallbone, P. Mendes, Metabolic regulation is sufficient for global and robust coordination of glucose uptake, catabolism, energy production and growth in Escherichia coli. *PLoS Comput. Biol.* **13**, e1005396 (2017).
45. M. Chen *et al.*, MTBLS6444: Glycolytic *flux* in *yeast* is increased by decreasing metabolite regulation and lowering *protein* phosphorylation. *MetaboLights*. www.ebi.ac.uk/metabolights/MTBLS6444. 2023-11-11.
46. J. Xia *et al.*, *Proteome* allocation of budding *yeast* under different growth rates. *Proteomics Identification Database*. https://www.ebi.ac.uk/pride/archive/projects/PXD012891. 2021-08-09.